

# Multifunctional Noble Metal Phosphide Electrocatalysts for Organic Molecule Electro-Oxidation

Zhipeng Yu, Xian-Kui Wei, Junyuan Xu, Yue Li, Ana Araujo, Joaquim L. Faria, Rafal E. Dunin-Borkowski, and Lifeng Liu\*

Cite This: *ACS Appl. Energy Mater.* 2021, 4, 1593–1600

Read Online

ACCESS |

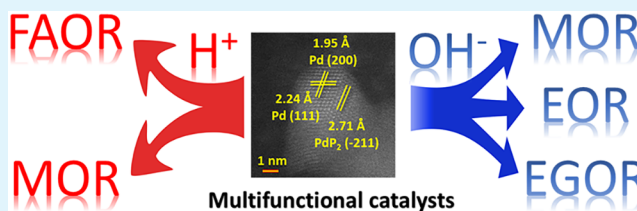
Metrics & More

Article Recommendations

Supporting Information

**ABSTRACT:** Small organic molecule electro-oxidation (OMEEO) is the important anodic reaction occurring in direct liquid fuel cells (DLFCs) and requires efficient and durable electrocatalysts to promote the reactivity and operational stability. Noble metals (e.g., Pt and Pd) are currently the state-of-the-art catalysts for OMEEO; however, for practical applications, their electrocatalytic performance needs to be improved. Herein, we report a simple and potentially cost-effective approach to the synthesis of noble metal phosphide ( $M_xP_y$ ,  $M = Pd, Pt$ ) catalysts, which is realized by phosphidating commercially available supported noble metal catalysts in red phosphorus vapor at different temperatures. We demonstrate that the derived  $PdP_2$ -Pd/C heterostructured catalysts show the best electrocatalytic performance toward a number of OMEEO model reactions, including the formic acid oxidation reaction, methanol oxidation reaction, ethanol oxidation reaction, and ethylene glycol oxidation reaction, in terms of not only apparent activity but also of specific and mass activities, poisoning tolerance, and catalytic stability, with respect to both the starting Pd/C and other prepared palladium phosphide control catalysts. Similar performance enhancement is also observed for the  $PtP_2$ -Pt/C heterostructured catalysts for all model reactions. The enhancement may result from the synergy between the noble metal phosphide and the noble metal, where the formed phosphide facilitates the adsorption of hydroxyl species and promotes the oxidation of poisoning intermediates, giving rise to improved activity, poisoning tolerance, and stability. Our work demonstrates an easy way of boosting the electrocatalytic performance of commercial catalysts toward multiple OMEEO reactions and shows substantial promise for their usage in DLFCs.

**KEYWORDS:** noble metal phosphide, organic molecule electro-oxidation, multifunctionality, facile catalyst synthesis, fuel cell catalyst



## INTRODUCTION

The increasing global demand for sustainable energy and the aggravation of environmental problems have sparked extensive research interest in novel, efficient, and fossil fuel-free energy systems, such as fuel cells that can directly convert chemical energy into electricity. Fuel cells can be used as both primary and backup power in a number of applications including fuel cell vehicles and are expected to play a key role in the current transition to a sustainable economy.<sup>1,2</sup> Among many types of fuel cells developed so far, the proton-exchange membrane fuel cell (PEMFC), which uses hydrogen as a fuel during its operation, is the most popular one.<sup>3</sup> However, the storage and transport of hydrogen along with the safety issues have been serious concerns for large-scale commercialization. Compared to PEMFC, direct liquid fuel cells (DLFCs), such as direct alcohol fuel cell<sup>4–8</sup> and direct formic acid fuel cell<sup>9,10</sup> using small molecules as a fuel (e.g., methanol,<sup>6</sup> ethanol,<sup>7</sup> ethylene glycol,<sup>8</sup> or formic acid<sup>9,10</sup>), offer a number of advantages including higher energy density, ease of storage and transport, and better safety.

Two half reactions usually occur in DLFCs, namely, the small organic molecule electro-oxidation (OMEEO) at the

anode and the oxygen reduction at the cathode. To improve the cell efficiency and expedite the reaction kinetics, usage of electrocatalysts to promote the OMEEO is in general indispensable. Platinum (Pt) and palladium (Pd) are by far the most commonly used anode electrocatalysts in DLFCs fed with low-molecular-weight alcohols.<sup>11–14</sup> However, the high price and low earth abundance of noble metals Pt and Pd impose a grand challenge for the market penetration of DLFCs.<sup>5,11</sup> In addition, the partially oxidized intermediates during the OMEEO, such as carbon monoxide (CO), even at ppm level, are known to be able to poison noble metal catalysts, causing a gradual performance degradation and eventually a failure.<sup>15,16</sup> Thus, considerable research effort has been dedicated to engineering the microstructure and composition of catalysts to improve the catalytic performance

Received: November 9, 2020

Accepted: January 21, 2021

Published: February 2, 2021



and lifetime toward the OMEO.<sup>5,12,17–19</sup> For example, many researchers were focused on the improved dispersion of Pt or Pd nanoparticles on a better catalyst support<sup>20–22</sup> and on the development of Pt- or Pd-based alloy catalysts such as noble metal alloys,<sup>23–25</sup> noble metal–transition-metal alloys,<sup>26–28</sup> noble metal–oxide composites,<sup>29,30</sup> and noble metal compounds (e.g., PtP and PdP<sub>2</sub>).<sup>31–35</sup> Among these, noble metal phosphide catalysts stand out for their improved mass activity,<sup>31,32</sup> enhanced corrosion resistance, and poisoning tolerance,<sup>33–37</sup> which have recently drawn significant research interest. In addition, from the application perspective, it is highly desirable for one single catalyst to be active toward several OMEO reactions, such as formic acid oxidation reaction (FAOR),<sup>26,28,35–37</sup> methanol oxidation reaction (MOR),<sup>20,22–24,26,30,31,33,36</sup> ethanol oxidation reaction (EOR),<sup>21,22,26–30,34,36</sup> and ethylene glycol oxidation reaction (EGOR),<sup>22,25,26,30,32,36</sup> to simplify the design and mass production of catalysts, satisfying the needs of different types of DLFCs. To this end, there are already some progresses recently on multifunctional OMEO catalysts,<sup>22,26,28,30,35,36</sup> but the breadth of multifunctionalities (e.g., the type of fuels oxidized and electrolytes used) and electrocatalytic performance toward each of the multiple reactions still need to be further improved.

Herein, we report the facile synthesis of palladium phosphide electrocatalysts with different microstructures and compositions (i.e., PdP<sub>2</sub>/C, PdP<sub>2</sub>–Pd/C, and Pd<sub>3</sub>P<sub>2</sub>–Pd/C) by the one-step phosphidation of commercially available Pd/C catalysts at different temperatures. Compared to the commercial Pd/C catalysts, the best-performing PdP<sub>2</sub>–Pd/C catalysts show markedly enhanced electrocatalytic performance toward all OMEO reactions of investigation, including the FAOR, MOR, EOR, and EGOR, in terms of not only the apparent activity but also poisoning tolerance, mass activity, specific activity, and catalytic stability. Furthermore, we demonstrate that the one-step phosphidation of commercial Pt/C catalysts also enables the formation of platinum phosphide catalysts (i.e., PtP<sub>2</sub>/C and PtP<sub>2</sub>–Pt/C), which enhances the electrocatalytic performance for the OMEO as well.

## EXPERIMENTAL SECTION

**Materials Synthesis.** The PdP<sub>2</sub>/C, PdP<sub>2</sub>–Pd/C, and Pd<sub>3</sub>P<sub>2</sub>–Pd/C catalysts were prepared by directly phosphorizing commercial Pd/C powders (20 wt % Pd, FuelCellStore, product code: 3151611) at 430, 500, and 700 °C, respectively, using red P as the source of phosphorus.<sup>38</sup> Similarly, PtP<sub>2</sub>/C and PtP<sub>2</sub>–Pt/C catalysts were synthesized by phosphorizing commercial Pt/C powders (30 wt % Pt, FuelCellStore, product code: 591378) at 500 and 700 °C, respectively, in the red P vapor. First, 20 mg of commercial Pd/C or Pt/C was placed in a ceramic boat, whereas 200 mg of red P was loaded 2 cm away from the catalysts at the upstream side. Then, the boat was transferred into a tube furnace, with high-purity N<sub>2</sub> (99.999%) purged at a flow rate of 800 sccm for 1 h before heating. The furnace was subsequently ramped to a given temperature at a rate of 10 °C min<sup>–1</sup>, held at this temperature for 2 h, and then cooled down naturally to room temperature. A constant N<sub>2</sub> flow was maintained throughout the whole process.

**Material Characterization.** X-ray diffractometry (XRD) experiments were conducted on an X'Pert PRO diffractometer (PANalytical) set at 45 kV and 40 mA, using Cu K $\alpha$  radiation ( $\lambda = 1.541874$  Å) and a PIXcel detector. Data were collected with the Bragg–Brentano configuration in the  $2\theta$  range of 20–100° at a scan speed of 0.011° s<sup>–1</sup>. X-ray photoelectron spectroscopy (XPS) characterization was carried out on an ESCALAB 250 instrument

with Al K $\alpha$  X-rays (1486.6 eV). Scanning electron microscopy (SEM) examination was performed on a FEI Quanta 650 FEG microscope equipped with an INCA 350 spectrometer (Oxford Instruments) for energy-dispersive X-ray spectroscopy (EDX) analysis. Transmission electron microscopy (TEM) and high-angle annular dark field scanning transmission electron microscopy (HAADF-STEM) investigations were conducted on a probe-corrected transmission electron microscope FEI ChemiSTEM 80-200 operated at 200 kV.

**Electrochemical Measurements.** All the electrochemical tests were performed in a three-electrode system at room temperature using a Biologic VMP-3 potentiostat/galvanostat. A glass carbon (GC) was utilized as the working electrode, whereas a saturated calomel electrode (SCE) and a graphite rod were used as the reference and the counter electrode, respectively. Prior to each measurement, the SCE reference electrode was calibrated in Ar/H<sub>2</sub>-saturated 0.5 M H<sub>2</sub>SO<sub>4</sub> solution using a clean Pt wire as the working electrode. The catalysts (5 mg) and Nafion solution (50  $\mu$ L) (Sigma, 5 wt %) were dispersed into 950  $\mu$ L of ethanol. Subsequently, 20  $\mu$ L of ink was loaded onto the polished glassy carbon electrode with an exposed area of 0.78 cm<sup>2</sup>, resulting in a loading density of 0.128 mg cm<sup>–2</sup>.

The electrocatalytic OMEO was tested using cyclic voltammetry (CV) at a scan rate of 20 mV s<sup>–1</sup>. The chronoamperometry (CA) measurements were conducted at 0.2 and 0.6 V versus SCE in 1.0 M HClO<sub>4</sub> + 0.5 M HCOOH and 0.1 M HClO<sub>4</sub> + 0.5 M CH<sub>3</sub>OH, respectively, in order to evaluate the catalytic stability of the FAOR and MOR in an acidic electrolyte (denoted as FAOR-H and MOR-H, respectively). Meanwhile, the catalytic durability of MOR, EOR, and EGOR in an alkaline electrolyte (denoted as MOR-OH, EOR-OH, and EGOR-OH, respectively) was tested at –0.3 V versus SCE using CA in 1.0 M KOH + 0.5 M CH<sub>3</sub>OH, 1.0 M KOH + 0.5 M CH<sub>3</sub>CH<sub>2</sub>OH, and 1.0 M KOH + 0.5 M EG, respectively.

The electrochemical surface areas (ECSAs) of Pd-based electrocatalysts were calculated based on the integrated charges in the reduction region of PdO in N<sub>2</sub>-purged 0.1 M HClO<sub>4</sub>, 1.0 M HClO<sub>4</sub>, or 1.0 M KOH solution using the following equation, in which the value of the charge density of the reduction of a PdO monolayer on the catalyst surface is assumed to be  $C_0 = 405 \mu\text{C cm}^{-2}$  according to a previous report<sup>34</sup>

$$\text{ECSA} = Q/m_{\text{metal}}C_0 \quad (1)$$

The ECSA of Pt-based electrocatalysts was computed using the same formula by integrating the charge associated with H desorption in N<sub>2</sub>-purged 0.1 M HClO<sub>4</sub>, 1.0 M HClO<sub>4</sub>, or 1.0 M KOH solution in the range of the hydrogen adsorption–desorption ( $Q_{\text{H}}$ ) regions, in which the value of the charge density related to a monolayer of hydrogen adsorbed on platinum is assigned to be  $C_0 = 210 \mu\text{C cm}^{-2}$ .<sup>39,40</sup>

In eq 1,  $Q$  represents the integral charge in the reduction region of PdO or the charge associated with the H desorption of Pt, and  $m_{\text{metal}}$  stands for the mass of Pd or Pt loaded on the electrode surface.

## RESULTS AND DISCUSSION

According to the P–Pd<sup>41</sup> and P–Pt<sup>42</sup> phase diagrams, Pd and Pt are easy to react with P, forming phosphides, even in the presence of a small amount of phosphorus (e.g. 20–30 at. %), at comparatively low temperatures.<sup>41</sup> Moreover, the stoichiometry of the formed phosphide is dependent on the ratio of the metal and P fed for the reaction. Our XRD examination revealed that by changing the phosphidation temperature, palladium phosphide with different phase structures can be obtained. For example, for the sample phosphorized at 430 °C (i.e., PdP<sub>2</sub>/C), diffraction peaks exclusively from the PdP<sub>2</sub> phase (ICDD no. 04-007-1929) were observed and those from metallic Pd disappeared (Figure 1a), indicating that Pd was completely converted into PdP<sub>2</sub>. As the temperature was increased to 500 °C, diffractions from both PdP<sub>2</sub> and metallic Pd (as evidenced by the broadened bump centered at 40.1°)

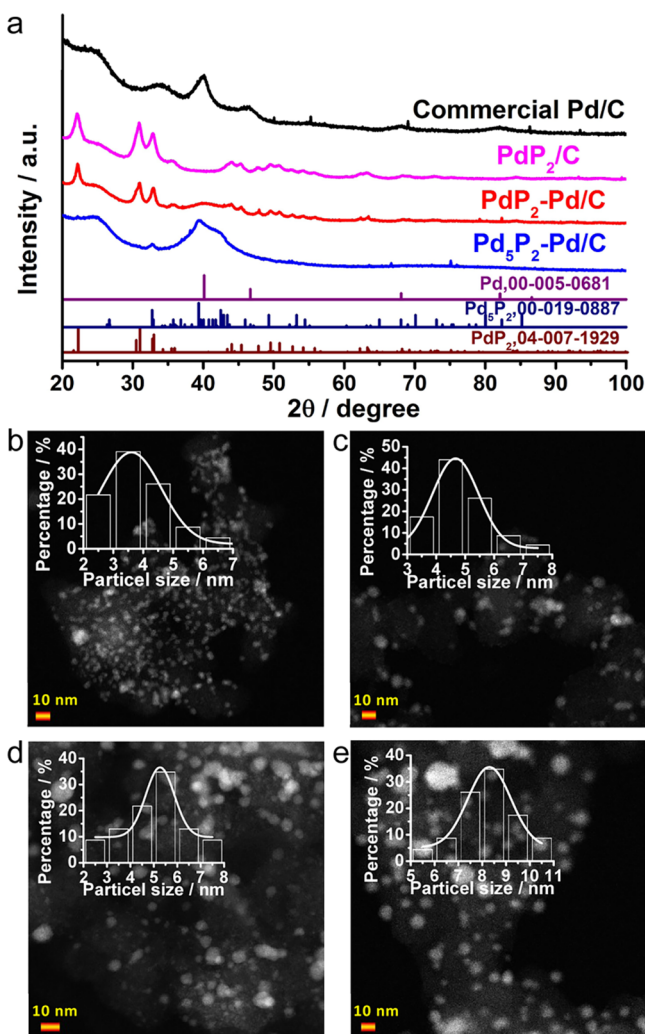


**Figure 1.** (a) XRD patterns of commercial Pd/C, the obtained PdP<sub>2</sub>/C, PdP<sub>2</sub>-Pd/C, and Pd<sub>5</sub>P<sub>2</sub>-Pd/C catalysts. HAADF-STEM images of (b) commercial Pd/C, (c) PdP<sub>2</sub>/C, (d) PdP<sub>2</sub>-Pd/C, and (e) Pd<sub>5</sub>P<sub>2</sub>-Pd/C. Insets of (b–e): histograms showing the nanoparticle size distribution.

were visible, with PdP<sub>2</sub> as the dominant phase (denoted as PdP<sub>2</sub>-Pd/C). The coexistence of PdP<sub>2</sub> and Pd suggests that Pd is partially phosphorized into PdP<sub>2</sub>, which was corroborated by our HAADF-STEM imaging and XPS study, as will be discussed below. Further increasing the phosphidation temperature to 700 °C resulted in the formation of mixed phases of Pd<sub>5</sub>P<sub>2</sub> (ICDD no. 00-019-0887) and Pd (denoted as Pd<sub>5</sub>P<sub>2</sub>-Pd/C), characterized by a broad diffraction peak in the range of 35.3–46.1°. We believe that the temperature-dependent phase composition evolution results from the amount of P vapor available to react with Pd nanoparticles. At high temperatures, phosphorus has a high vapor pressure, and the generated P vapor would be rapidly carried away by the N<sub>2</sub> gas flow, such that Pd cannot be completely phosphorized, and the formed phosphide is Pd-rich. However, at comparatively low temperatures, the generated P vapor would have a longer dwell time because of the low vapor pressure, and therefore more P is available to react with Pd, forming a P-rich PdP<sub>2</sub> phase and enabling the complete conversion of Pd into phosphide. This is consistent with the phase distribution in the P–Pd phase diagram.<sup>41</sup>

The obtained palladium phosphide catalysts were characterized by SEM, and their morphology was found to be very similar to that of the commercial Pd/C starting materials (Figure S1). Furthermore, the dispersion of palladium phosphide nanoparticles on a carbon support was investigated by HAADF-STEM imaging. The average catalyst particle size of Pd/C is ca. 3.5 nm (Figure 1b), and the size was increased upon phosphidation, being 4.5 nm for PdP<sub>2</sub>/C (Figure 1c), 5.0 nm for PdP<sub>2</sub>-Pd/C (Figure 1d), and 8.0 nm for Pd<sub>5</sub>P<sub>2</sub>-Pd/C (Figure 1e).

The atomic structure of the palladium phosphide nanoparticles and the Pd/C control sample was further investigated by STEM in the HAADF mode. Lattice fringes with an interplanar spacing of 0.224 nm can be resolved for commercial Pd/C (Figure 2a), corresponding to the lattice

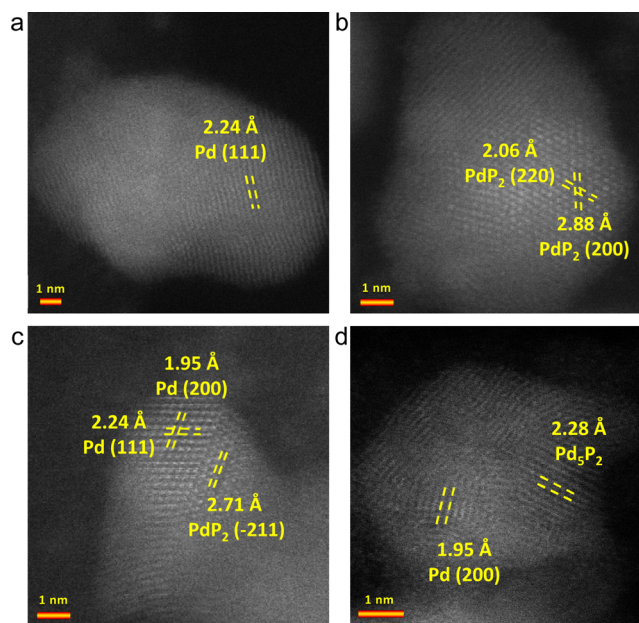


**Figure 2.** HAADF-STEM images of (a) commercial Pd/C, (b) PdP<sub>2</sub>/C, (c) PdP<sub>2</sub>-Pd/C, and (d) Pd<sub>5</sub>P<sub>2</sub>-Pd/C catalysts.

distance of Pd(111) crystal planes. For PdP<sub>2</sub>/C, the interplanar spacings of 0.206 and 0.288 nm correspond to the lattice distances of PdP<sub>2</sub> (220) and (200) crystal planes (Figure 2b), respectively. Moreover, the measured angle between these two planes (44.5°) is in good agreement with that calculated based on the monoclinic PdP<sub>2</sub> structure, corroborating the formation of PdP<sub>2</sub> phase. EDX mapping confirmed that both Pd and P are uniformly distributed over a single nanoparticle (Figure S2a), and no obvious segregation was observed. For PdP<sub>2</sub>-Pd/C obtained upon phosphidation at 500 °C, the lattice fringes from both PdP<sub>2</sub> and metallic Pd can be resolved (Figure 2c). EDX mapping revealed that the intensity of P is attenuated and the distribution of P does not completely overlap with that of Pd (Figure S2b), suggesting the partial phosphidation. Similar heterostructure and elemental distribution were also observed in Pd<sub>5</sub>P<sub>2</sub>-Pd/C (Figures 2d and S2c), but the intensity of P signal in this sample was even lower.

The surface composition and electronic structure of PdP<sub>2</sub>/C, PdP<sub>2</sub>-Pd/C, and Pd<sub>5</sub>P<sub>2</sub>-Pd/C were further studied by XPS and compared to those of commercial Pd/C control catalysts. The XPS survey spectra confirm the presence of the corresponding elements in each catalyst (Figure S3). Figure

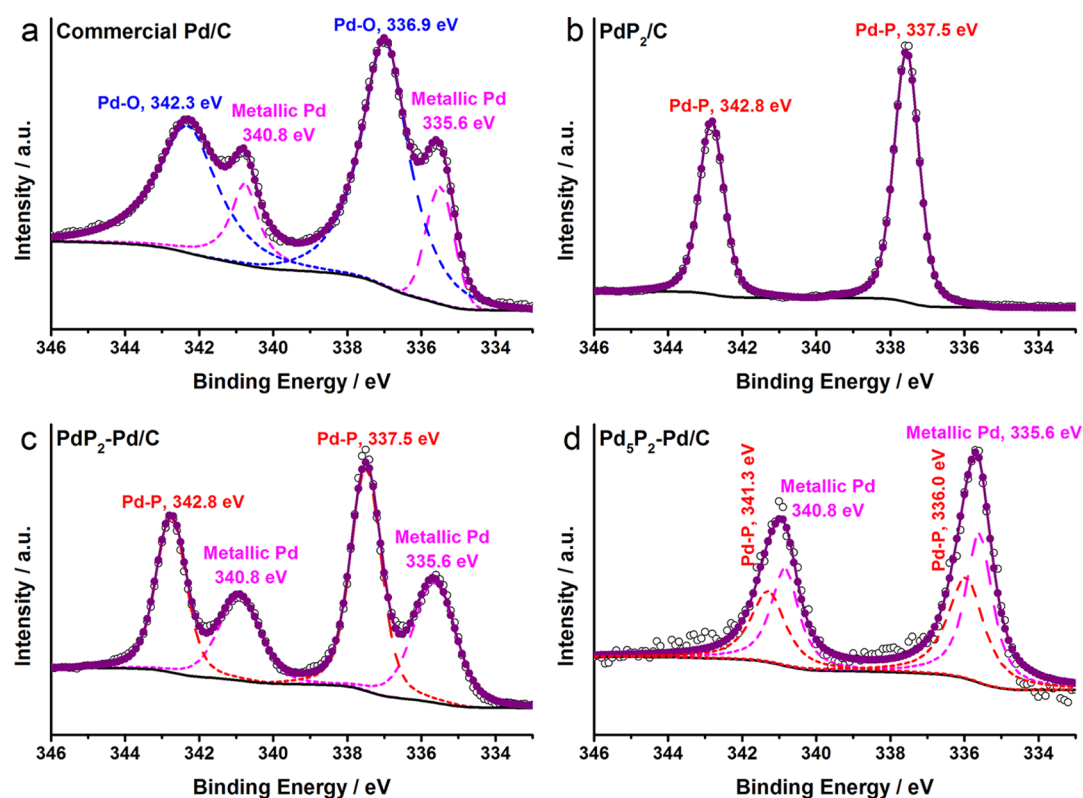


**Figure 3.** High-resolution Pd 3d XPS spectra of (a) commercial Pd/C, (b) PdP<sub>2</sub>/C, (c) PdP<sub>2</sub>-Pd/C, and (d) Pd<sub>5</sub>P<sub>2</sub>-Pd/C catalysts.

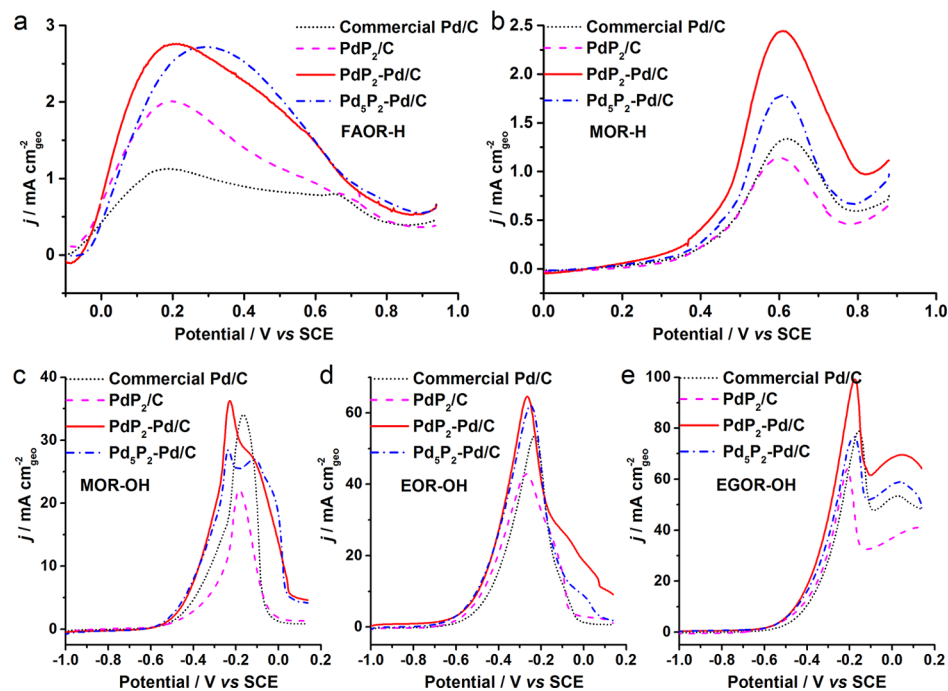


**Figure 4.** Electro-oxidation performance of commercial Pd/C, PdP<sub>2</sub>/C, PdP<sub>2</sub>-Pd/C, and Pd<sub>5</sub>P<sub>2</sub>-Pd/C catalysts toward different OMEO reactions. (a) FAOR-H recorded in 0.5 M HCOOH + 1.0 M HClO<sub>4</sub>. (b) MOR-H recorded in 0.5 M CH<sub>3</sub>OH + 0.1 M HClO<sub>4</sub>. (c) MOR-OH recorded in 1.0 M CH<sub>3</sub>OH + 1.0 M KOH. (d) EOR-OH recorded in 1.0 M CH<sub>3</sub>CH<sub>2</sub>OH + 1.0 M KOH. (e) EGOR-OH recorded in 1.0 M EG + 1.0 M KOH. All CV curves were recorded at 20 mV s<sup>-1</sup>.

3 shows the Pd 3d XPS spectra of all samples, where the two components assigned to Pd 3d<sub>5/2</sub> and Pd 3d<sub>3/2</sub> can be resolved. For commercial Pd/C, four binding energy (BE) peaks can be deconvoluted (Figure 3a): the ones appearing at 335.6 and 340.8 eV can be assigned to Pd<sup>0</sup> and those at 336.9 and 342.3

eV to the Pd–O bonding, which arise from the surface oxidation of Pd/C. Upon phosphidation at 430 °C, the BE peaks from both Pd<sup>0</sup> and Pd–O disappeared, and new peaks at 337.5 and 342.8 eV, characteristic of Pd<sup>2+</sup> in palladium phosphide,<sup>43</sup> appeared (Figure 3b), indicating the complete

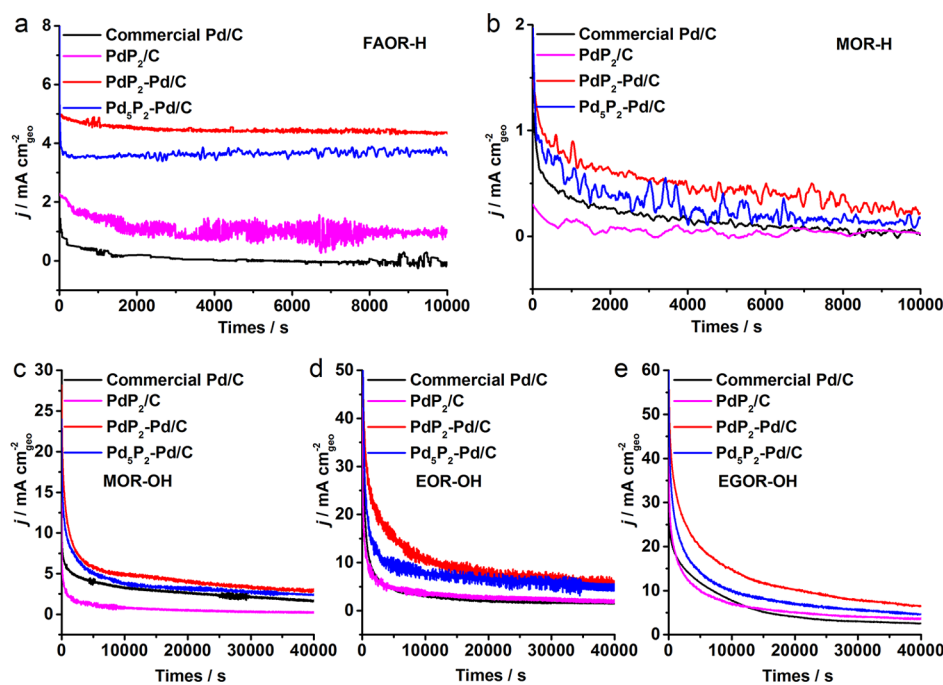


**Figure 5.** Stability of commercial Pd/C, PdP<sub>2</sub>/C, PdP<sub>2</sub>-Pd/C, and Pd<sub>5</sub>P<sub>2</sub>-Pd/C catalysts. CA curves measured in (a) 0.5 M HCOOH + 1.0 M HClO<sub>4</sub> solution at 0.2 V vs SCE; (b) 0.5 M CH<sub>3</sub>OH + 0.1 M HClO<sub>4</sub> solution at 0.6 V vs SCE; (c) 1.0 M CH<sub>3</sub>OH + 1.0 M KOH; (d) 1.0 M CH<sub>3</sub>CH<sub>2</sub>OH + 1.0 M KOH; and (e) 1.0 M EG + 1.0 M KOH solution at -0.3 V vs SCE.

phosphidation of Pd.<sup>34</sup> For PdP<sub>2</sub>-Pd/C, in addition to the Pd-P characteristic peaks, the BE peaks that can be assigned to Pd<sup>0</sup> were also observed (Figure 3c), implying the partial phosphidation at 500 °C. Furthermore, for Pd<sub>5</sub>P<sub>2</sub>-Pd/C obtained at 700 °C, we found the components from both Pd<sup>0</sup> and Pd-P (Figure 3d). However, the BE peaks from Pd-P show a lower intensity compared to those from Pd<sup>0</sup> and a red shift with respect to the peaks of PdP<sub>2</sub> (Figure 3d), which suggest that the degree of phosphating in this sample is low and the oxidation state of Pd should be below 2+. This agrees well with the identification of the Pd<sub>5</sub>P<sub>2</sub>-Pd structure, as revealed by our XRD and TEM results discussed above.

In addition, in the P 2p spectra of all palladium phosphide catalysts (Figure S4), there are two BE peaks located at 129.7 and 130.6 eV, which can be assigned to the 2p<sub>3/2</sub> and 2p<sub>1/2</sub> core levels of P atoms, characteristic of metal phosphides.<sup>44</sup> Another peak appearing at 133.4 eV is assigned to the oxidized phosphorus species resulting from the oxidation upon contact with air.<sup>38,45</sup> It is interesting to note that the intensity ratio of Pd-P characteristic peaks over phosphate characteristic peaks decreases in the following order: PdP<sub>2</sub>/C > PdP<sub>2</sub>-Pd/C > Pd<sub>5</sub>P<sub>2</sub>-Pd/C, implying that the phosphidation degree decreases as the phosphidation temperature increases, which agrees with the XRD and TEM data as well as the XPS Pd 3d spectra.

The OMEO electrocatalytic activities of commercial Pd/C, PdP<sub>2</sub>/C, PdP<sub>2</sub>-Pd/C, and Pd<sub>5</sub>P<sub>2</sub>-Pd/C were investigated toward several model reactions including FAOR-H, MOR-H, MOR-OH, EOR-OH, and EGOR-OH. Figure 4a displays the linear scan voltammograms (i.e., forward scan curves) of the catalysts for FAOR-H in 0.5 M HCOOH + 1.0 M HClO<sub>4</sub>, and the cyclic voltammograms (i.e., forward and reverse scans) of the catalysts are shown in Figure S5. The apparent peak current density of PdP<sub>2</sub>-Pd/C is 2.76 mA cm<sub>geo</sub><sup>-2</sup> at 0.21 V versus SCE, outperforming Pd<sub>5</sub>P<sub>2</sub>-Pd/C (2.72 mA cm<sub>geo</sub><sup>-2</sup>),

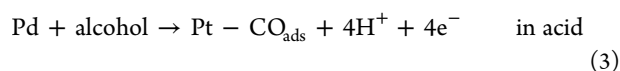
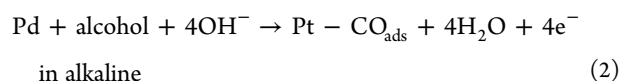
PdP<sub>2</sub>/C (2.02 mA cm<sub>geo</sub><sup>-2</sup>), and commercial Pd/C (1.13 mA cm<sub>geo</sub><sup>-2</sup>). For MOR-H, the PdP<sub>2</sub>-Pd/C catalyst delivers an apparent peak current density of 2.44 mA cm<sub>geo</sub><sup>-2</sup> at 0.61 V versus SCE (Figure 4b), 1.4, 2.1, and 1.8 times that of the Pd<sub>5</sub>P<sub>2</sub>-Pd/C, PdP<sub>2</sub>/C, and commercial Pd/C, respectively. For the OMEO taking place in alkaline solution (Figure 4c-e), PdP<sub>2</sub>-Pd/C can deliver geometric peak current densities of 36.3, 64.6, and 99.3 mA cm<sub>geo</sub><sup>-2</sup> for MOR-OH, EOR-OH, and EGOR-OH, respectively, substantially higher than those of Pd<sub>5</sub>P<sub>2</sub>-Pd/C (28.5, 62.0, and 76.6 mA cm<sub>geo</sub><sup>-2</sup>), PdP<sub>2</sub>/C (22.1, 43.0, and 64.1 mA cm<sub>geo</sub><sup>-2</sup>), and commercial Pd/C reference catalysts (34.0, 53.5, and 78.9 mA cm<sub>geo</sub><sup>-2</sup>) tested under the same conditions.

To assess the intrinsic catalytic performance, the ECSA-normalized specific activities of PdP<sub>2</sub>-Pd/C and other control catalysts, which reflect the reactivity of each active site, were calculated and compared. The ECSAs were calculated by CV measurements in the acidic/alkaline electrolyte used for each model reaction (see Experimental Section and Figure S6). PdP<sub>2</sub>-Pd/C exhibits the highest ECSA with respect to that of other control catalysts in all the three electrolytes used (i.e., 1.0 M HClO<sub>4</sub>, 0.1 M HClO<sub>4</sub>, and 1.0 M KOH), suggesting that the introduction of P is conducive to the exposure of more catalytically active sites. Nevertheless, after normalization, PdP<sub>2</sub>-Pd/C still shows the highest specific activity, followed by Pd<sub>5</sub>P<sub>2</sub>-Pd/C, PdP<sub>2</sub>/C, and commercial Pd/C for all the reactions (Figure S7), indicating that PdP<sub>2</sub>-Pd/C is intrinsically more active than all other control catalysts.

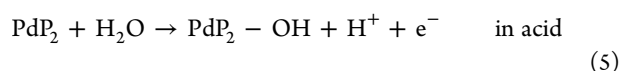
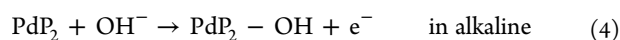
The mass activities of all catalysts, which is an important consideration from the cost perspective for practical applications, were also calculated and compared in Figure S8. All palladium phosphide catalysts show enhanced mass activities higher than that of the starting Pd/C catalysts, following the order of PdP<sub>2</sub>-Pd/C > Pd<sub>5</sub>P<sub>2</sub>-Pd/C > PdP<sub>2</sub>/C > Pd/C. This illustrates that the introduction of phosphorus

into Pd markedly improves the degree of utilization of noble metal Pd. In addition, PdP<sub>2</sub>-Pd/C also shows a more negative onset potential and a relatively large current density at a given low oxidation potential toward all OMEO reactions under investigation (Table S1), suggesting that OMEO is likely easier to occur on the surface of PdP<sub>2</sub>-Pd/C.

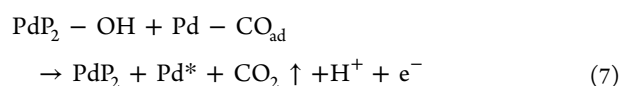
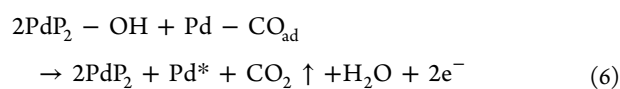
According to the above discussion, PdP<sub>2</sub>-Pd/C, obtained by the phosphidation of Pd/C at 500 °C, exhibits the best electrocatalytic performance in terms of apparent, mass, and specific activities. We believe that the ensemble effect might be essential for PdP<sub>2</sub>-Pd/C to achieve an enhanced catalytic performance. It is known that \*CO is an intermediate that is generally produced during the oxidation of formic acid and C1/C2 alcohols,<sup>11,12</sup> which would cause a serious degradation in the activity and lifetime of electrocatalysts. For our PdP<sub>2</sub>-Pd/C catalysts, we presume that the poisoning \*CO intermediate is mainly absorbed on the metallic Pd surface during the alcohol dehydrogenation, as described in the following equations



On the other hand, the presence of phosphorus in PdP<sub>2</sub> is likely to facilitate the adsorption of hydroxyl species at low potentials,<sup>37</sup> and the following process may happen



Once PdP<sub>2</sub>-OH is formed, the poisoning \*CO intermediate absorbed on the neighboring active Pd sites can be oxidized to CO<sub>2</sub>, leaving fresh Pd active sites for the subsequent new catalytic cycles, as described below in eqs 6 and 7, which is similar to the bifunctional mechanism reported for Pt-Ru catalysts toward the MOR.<sup>5,15</sup>



In this case, the poisoning tolerance would also be enhanced, and this was indeed observed for PdP<sub>2</sub>-Pd/C toward all OMEO reactions under investigation with respect to the Pd/C catalysts (Table S2).

Stability is a critically important indicator of electrocatalysts for practical applications in DLFCs. We have examined the catalytic stability of all catalysts for each model reaction using CA. As shown in Figure 5, PdP<sub>2</sub>-Pd/C turns out to be the best-performing electrocatalyst, although all of the catalysts show a decreased activity over time, which was commonly observed in nearly all previously reported Pd-based electrocatalysts.<sup>5,12,17,34,37</sup> The enhanced stability of PdP<sub>2</sub>-Pd/C catalysts could result from the improved poisoning tolerance. Besides, metal phosphides might activate water and be prone to adsorbing -OH<sub>ads</sub> species, which may oxidize the poisoning intermediates around the active sites, thereby prolonging the

life of the catalysts.<sup>37</sup> The enhanced activity and stability will be beneficial for future practical applications in DLFCs.

In addition to palladium phosphide, we demonstrated that the simple one-step phosphidation treatment can also be extended to synthesize supported platinum phosphide catalysts (e.g., PtP<sub>2</sub>/C and PtP<sub>2</sub>-Pt/C) using commercially available Pt/C as the starting materials. The XRD, XPS, and TEM results confirmed the formation of PtP<sub>2</sub>/C and PtP<sub>2</sub>-Pt/C at different phosphidation temperatures, as illustrated in Figures S9-S12. Furthermore, we proved that upon phosphidation treatment, the electrocatalytic performance of the obtained PtP<sub>2</sub>-Pt/C catalysts showed obvious enhancement in terms of not only the apparent activity but also specific and mass activities, as well as poisoning tolerance (Table S2), for almost all model reactions (Figures S13-S15), similar to the results we obtained for palladium phosphide catalysts, highlighting that phosphidation is an effective and generic strategy for improving the catalytic OMEO performance of commercial noble metal catalysts.

## CONCLUSIONS

In summary, we demonstrate that a simple phosphidation treatment at different temperatures is able to convert commercial noble metal nanoparticles into metal phosphides or phosphide-metal heterostructures. Typically, the PdP<sub>2</sub>-Pd/C catalysts obtained by phosphidating commercial Pd/C at 500 °C show markedly improved electrocatalytic performance toward a number of small OMEO reactions, in terms of not only apparent catalytic activity but also of specific and mass activities, poisoning tolerance, and catalytic stability, showing preferable multifunctionalities. The enhanced performance likely results from the synergy between PdP<sub>2</sub> and Pd, in which PdP<sub>2</sub> facilitates the adsorption of hydroxyl species, promoting the oxidation of the poisonous \*CO intermediates, leading to improved activity and durability. We also demonstrate the applicability of the one-step phosphidation to synthesizing multifunctional platinum phosphide catalysts. Our study provides a new, simple, and potentially cost-effective approach to improving the electrocatalytic performance of commercial catalysts for use in DLFCs.

## ASSOCIATED CONTENT

### Supporting Information

The Supporting Information is available free of charge at <https://pubs.acs.org/doi/10.1021/acsaem.0c02803>.

SEM, HAADF-STEM images, XPS, and electrocatalytic performance of commercial Pd/C, PdP<sub>2</sub>/C, PdP<sub>2</sub>-Pd/C, and Pd<sub>3</sub>P<sub>2</sub>-Pd/C catalysts; XRD, XPS, TEM, and electrocatalytic performance of commercial Pt/C, PtP<sub>2</sub>/C, and PtP<sub>2</sub>-Pt/C catalysts; and comparison of the electrocatalytic activity and poisoning tolerance of different catalysts (PDF)

## AUTHOR INFORMATION

### Corresponding Author

Lifeng Liu – International Iberian Nanotechnology Laboratory (INL), 4715-330 Braga, Portugal; [orcid.org/0000-0003-2732-7399](https://orcid.org/0000-0003-2732-7399); Email: [lifeng.liu@inl.int](mailto:lifeng.liu@inl.int)

### Authors

Zhipeng Yu – International Iberian Nanotechnology Laboratory (INL), 4715-330 Braga, Portugal; Laboratory of

Separation and Reaction Engineering Laboratory of Catalysis and Materials (LSRE-LCM), Faculdade de Engenharia, Universidade do Porto, 4200-465 Porto, Portugal

Xian-Kui Wei – Ernst Ruska-Centre for Microscopy and Spectroscopy with Electrons, Forschungszentrum Jülich GmbH, Jülich 52428, Germany; [orcid.org/0000-0003-4320-1120](https://orcid.org/0000-0003-4320-1120)

Junyuan Xu – International Iberian Nanotechnology Laboratory (INL), 4715-330 Braga, Portugal

Yue Li – International Iberian Nanotechnology Laboratory (INL), 4715-330 Braga, Portugal

Ana Araujo – International Iberian Nanotechnology Laboratory (INL), 4715-330 Braga, Portugal; Laboratory of Separation and Reaction Engineering Laboratory of Catalysis and Materials (LSRE-LCM), Faculdade de Engenharia, Universidade do Porto, 4200-465 Porto, Portugal

Joaquim L. Faria – Laboratory of Separation and Reaction Engineering Laboratory of Catalysis and Materials (LSRE-LCM), Faculdade de Engenharia, Universidade do Porto, 4200-465 Porto, Portugal; [orcid.org/0000-0002-6531-3978](https://orcid.org/0000-0002-6531-3978)

Rafal E. Dunin-Borkowski – Ernst Ruska-Centre for Microscopy and Spectroscopy with Electrons, Forschungszentrum Jülich GmbH, Jülich 52428, Germany; [orcid.org/0000-0001-8082-0647](https://orcid.org/0000-0001-8082-0647)

Complete contact information is available at: <https://pubs.acs.org/10.1021/acsaem.0c02803>

## Notes

The authors declare no competing financial interest.

## ACKNOWLEDGMENTS

The authors acknowledge the support of the TACIT project funded by Fundação para a Ciência e a Tecnologia, Portugal (grant no. PTDC/NAN-OPT/28837/2017). This project was also partially funded by the “Baterias 2030” project under the Mobilizador Programme by the National Innovation Agency of Portugal (grant no. POCI-01-0247-FEDER-046109). Z.Y. is grateful for the scholarship offered by the China Scholarship Council (grant no. 201806150015).

## REFERENCES

- (1) Staffell, I.; Scamman, D.; Velazquez Abad, A.; Balcombe, P.; Dodds, P. E.; Ekins, P.; Shah, N.; Ward, K. R. The role of hydrogen and fuel cells in the global energy system. *Energy Environ. Sci.* **2019**, *12*, 463–491.
- (2) Acres, G. Recent advances in fuel cell technology and its applications. *J. Power Sources* **2001**, *100*, 60–66.
- (3) Li, J.; Brüller, S.; Sabarirajan, D. C.; Ranjbar-Sahraie, N.; Sougrati, M. T.; Cavaliere, S.; Jones, D.; Zenyuk, I. V.; Zitolo, A.; Jaouen, F. Designing the 3D Architecture of PGM-Free Cathodes for H<sub>2</sub>/Air Proton Exchange Membrane Fuel Cells. *ACS Appl. Energy Mater.* **2019**, *2*, 7211–7222.
- (4) Antolini, E.; Gonzalez, E. R. Alkaline direct alcohol fuel cells. *J. Power Sources* **2010**, *195*, 3431–3450.
- (5) Bianchini, C.; Shen, P. K. Palladium-Based Electrocatalysts for Alcohol Oxidation in Half Cells and in Direct Alcohol Fuel Cells. *Chem. Rev.* **2009**, *109*, 4183–4206.
- (6) Zhao, X.; Yin, M.; Ma, L.; Liang, L.; Liu, C.; Liao, J.; Lu, T.; Xing, W. Recent advances in catalysts for direct methanol fuel cells. *Energy Environ. Sci.* **2011**, *4*, 2736–2753.

- (7) Zhou, W.; Zhou, Z. H.; Song, S. Q.; Li, W. Z.; Sun, G. Q.; Tsiakaras, P.; Xin, Q. Pt based anode catalysts for direct ethanol fuel cells. *Appl. Catal., B* **2003**, *46*, 273–285.

- (8) Serov, A.; Kwak, C. Recent achievements in direct ethylene glycol fuel cells (DEGFC). *Appl. Catal., B* **2010**, *97*, 1–12.

- (9) Yu, X.; Pickup, P. G. Recent advances in direct formic acid fuel cells (DFAFC). *J. Power Sources* **2008**, *182*, 124–132.

- (10) Rice, C.; Ha, S.; Masel, R. I.; Waszczuk, P.; Wieckowski, A.; Barnard, T. Direct formic acid fuel cells. *J. Power Sources* **2002**, *111*, 83–89.

- (11) Ren, X.; Lv, Q.; Liu, L.; Liu, B.; Wang, Y.; Liu, A.; Wu, G. Current progress of Pt and Pt-based electrocatalysts used for fuel cells. *Sustainable Energy Fuels* **2020**, *4*, 15–30.

- (12) Antolini, E. Palladium in fuel cell catalysis. *Energy Environ. Sci.* **2009**, *2*, 915–931.

- (13) Liu, L.; Pippel, E.; Scholz, R.; Gösele, U. Nanoporous Pt-Co alloy nanowires: fabrication, characterization, and electrocatalytic properties. *Nano Lett.* **2009**, *9*, 4352–4358.

- (14) Liu, L.; Scholz, R.; Pippel, E.; Gösele, U. Microstructure, electrocatalytic and sensing properties of nanoporous Pt<sub>46</sub>Ni<sub>54</sub> alloy nanowires fabricated by mild dealloying. *J. Mater. Chem.* **2010**, *20*, 5621–5627.

- (15) Xu, C.; Wang, L.; Mu, X.; Ding, Y. Nanoporous PtRu Alloys for Electrocatalysis. *Langmuir* **2010**, *26*, 7437–7443.

- (16) Hu, F.; Chen, C.; Wang, Z.; Wei, G.; Shen, P. K. Mechanistic study of ethanol oxidation on Pd–NiO/C electrocatalyst. *Electrochim. Acta* **2006**, *52*, 1087–1091.

- (17) Wang, R.; Liao, S.; Ji, S. High performance Pd-based catalysts for oxidation of formic acid. *J. Power Sources* **2008**, *180*, 205–208.

- (18) Long, G.-f.; Li, X.-h.; Wan, K.; Liang, Z.-x.; Piao, J.-h.; Tsiakaras, P. Pt/CN-doped electrocatalysts: Superior electrocatalytic activity for methanol oxidation reaction and mechanistic insight into interfacial enhancement. *Appl. Catal., B* **2017**, *203*, 541–548.

- (19) Li, D.; Wang, C.; Strmcnik, D. S.; Tripkovic, D. V.; Sun, X.; Kang, Y.; Chi, M.; Snyder, J. D.; van der Vliet, D.; Tsai, Y.; Stamenkovic, V. R.; Sun, S.; Markovic, N. M. Functional links between Pt single crystal morphology and nanoparticles with different size and shape: the oxygen reduction reaction case. *Energy Environ. Sci.* **2014**, *7*, 4061–4069.

- (20) Zhang, X.; Zhang, J.; Huang, H.; Jiang, Q.; Wu, Y. Platinum nanoparticles anchored on graphene oxide-dispersed pristine carbon nanotube supports: High-performance electrocatalysts toward methanol electrooxidation. *Electrochim. Acta* **2017**, *258*, 919–926.

- (21) Zheng, H. T.; Li, Y.; Chen, S.; Shen, P. K. Effect of support on the activity of Pd electrocatalyst for ethanol oxidation. *J. Power Sources* **2006**, *163*, 371–375.

- (22) Sankar, S.; Watanabe, N.; Anilkumar, G. M.; Nair, B. N.; Sivakamiammal, S. G.; Tamaki, T.; Yamaguchi, T. Electro-oxidation competency of palladium nanocatalysts over ceria–carbon composite supports during alkaline ethylene glycol oxidation. *Catal. Sci. Technol.* **2019**, *9*, 493–501.

- (23) Bai, L. Synthesis of PtRu/Ru heterostructure for efficient methanol electrooxidation: The role of extra Ru. *Appl. Surf. Sci.* **2018**, *433*, 279–284.

- (24) Zhang, J.; Huang, M.; Ma, H.; Tian, F.; Pan, W.; Chen, S. High catalytic activity of nanostructured Pd thin films electrochemically deposited on polycrystalline Pt and Au substrates towards electro-oxidation of methanol. *Electrochem. Commun.* **2007**, *9*, 1298–1304.

- (25) Shi, Y.-C.; Feng, J.-J.; Lin, X.-X.; Zhang, L.; Yuan, J.; Zhang, Q.-L.; Wang, A.-J. One-step hydrothermal synthesis of three-dimensional nitrogen-doped reduced graphene oxide hydrogels anchored PtPd alloyed nanoparticles for ethylene glycol oxidation and hydrogen evolution reactions. *Electrochim. Acta* **2019**, *293*, 504–513.

- (26) Chaudhari, N. K.; Hong, Y.; Kim, B.; Choi, S.-I.; Lee, K. Pt–Cu based nanocrystals as promising catalysts for various electrocatalytic reactions. *J. Mater. Chem. A* **2019**, *7*, 17183–17203.

- (27) Singh, R. N.; Singh, A.; Anindita. Electrocatalytic activity of binary and ternary composite films of Pd, MWCNT, and Ni for

ethanol electro-oxidation in alkaline solutions. *Carbon* **2009**, *47*, 271–278.

(28) Sankar, S.; Anilkumar, G. M.; Tamaki, T.; Yamaguchi, T. Cobalt-Modified Palladium Bimetallic Catalyst: A Multifunctional Electrocatalyst with Enhanced Efficiency and Stability toward the Oxidation of Ethanol and Formate in Alkaline Medium. *ACS Appl. Energy Mater.* **2018**, *1*, 4140–4149.

(29) Antoniassi, R. M.; Silva, J. C. M.; Oliveira Neto, A.; Spinacé, E. V. Synthesis of Pt+SnO<sub>2</sub>/C electrocatalysts containing Pt nanoparticles with preferential (100) orientation for direct ethanol fuel cell. *Appl. Catal., B* **2017**, *218*, 91–100.

(30) Xu, C.; Tian, Z.; Shen, P.; Jiang, S. P. Oxide (CeO<sub>2</sub>, NiO, Co<sub>3</sub>O<sub>4</sub> and Mn<sub>3</sub>O<sub>4</sub>)-promoted Pd/C electrocatalysts for alcohol electrooxidation in alkaline media. *Electrochim. Acta* **2008**, *53*, 2610–2618.

(31) Li, M.; Fang, Y.; Zhang, G.; Cui, P.; Yang, Z.; He, J. Carbon-supported Pt<sub>3</sub>P<sub>2</sub> nanoparticles used as a high-performance electrocatalyst for the methanol oxidation reaction. *J. Mater. Chem. A* **2020**, *8*, 10433–10438.

(32) Su, W.; Sun, R.; Ren, F.; Yao, Y.; Fei, Z.; Wang, H.; Liu, Z.; Xing, R.; Du, Y. Graphene supported palladium-phosphorus nanoparticles as a promising catalyst for ethylene glycol oxidation. *Appl. Surf. Sci.* **2019**, *491*, 735–741.

(33) Ma, Y.; Wang, H.; Li, H.; Key, J.; Ji, S.; Wang, R. Synthesis of ultrafine amorphous PtP nanoparticles and the effect of PtP crystallinity on methanol oxidation. *RSC Adv.* **2014**, *4*, 20722–20728.

(34) Liu, J.; Luo, Z.; Li, J.; Yu, X.; Llorca, J.; Nasioiu, D.; Arbiol, J.; Meyns, M.; Cabot, A. Graphene-supported palladium phosphide PdP<sub>2</sub> nanocrystals for ethanol electrooxidation. *Appl. Catal., B* **2019**, *242*, 258–266.

(35) Kucernak, A. R. J.; Fahy, K. F.; Sundaram, V. N. N. Facile synthesis of palladium phosphide electrocatalysts and their activity for the hydrogen oxidation, hydrogen evolutions, oxygen reduction and formic acid oxidation reactions. *Catal. Today* **2016**, *262*, 48–56.

(36) Yu, Z.; Xu, J.; Amorim, I.; Li, Y.; Liu, L. Easy preparation of multifunctional ternary PdNiP/C catalysts toward enhanced small organic molecule electro-oxidation and hydrogen evolution reactions. *J. Energy Chem.* **2021**, *58*, 256–263.

(37) Chang, J.; Feng, L.; Liu, C.; Xing, W.; Hu, X. An Effective Pd–Ni<sub>2</sub>P/C Anode Catalyst for Direct Formic Acid Fuel Cells. *Angew. Chem., Int. Ed.* **2014**, *53*, 122–126.

(38) Xu, J.; Xiong, D.; Amorim, I.; Liu, L. Template-Free Synthesis of Hollow Iron Phosphide–Phosphate Composite Nanotubes for Use as Active and Stable Oxygen Evolution Electrocatalysts. *ACS Appl. Nano Mater.* **2018**, *1*, 617–624.

(39) Zhan, D.; Velmurugan, J.; Mirkin, M. V. Adsorption/Desorption of Hydrogen on Pt Nanoelectrodes: Evidence of Surface Diffusion and Spillover. *J. Am. Chem. Soc.* **2009**, *131*, 14756–14760.

(40) Liu, L.; Huang, Z.; Wang, D.; Scholz, R.; Pippel, E. The fabrication of nanoporous Pt-based multimetallic alloy nanowires and their improved electrochemical durability. *Nanotechnology* **2011**, *22*, 105604.

(41) Okamoto, H. The P-Pd (phosphorus-palladium) system. *J. Phase Equilib.* **1994**, *15*, 58–61.

(42) Okamoto, H. The P-Pt (Phosphorus-Platinum) system. *J. Phase Equilib.* **1990**, *11*, 511–513.

(43) Xie, H.; Geng, Q.; Zhu, X.; Luo, Y.; Chang, L.; Niu, X.; Shi, X.; Asiri, A. M.; Gao, S.; Wang, Z.; Sun, X. PdP<sub>2</sub> nanoparticles–reduced graphene oxide for electrocatalytic N<sub>2</sub> conversion to NH<sub>3</sub> under ambient conditions. *J. Mater. Chem. A* **2019**, *7*, 24760–24764.

(44) Li, Y.; Wei, B.; Yu, Z.; Bondarchuk, O.; Araujo, A.; Amorim, I.; Zhang, N.; Xu, J.; Neves, I. C.; Liu, L. Bifunctional Porous Cobalt Phosphide Foam for High-Current-Density Alkaline Water Electrolysis with 4000-h Long Stability. *ACS Sustainable Chem. Eng.* **2020**, *8*, 10193–10200.

(45) Xu, J.; Liu, Y.; Li, J.; Amorim, I.; Zhang, B.; Xiong, D.; Zhang, N.; Thalluri, S. M.; Sousa, J. P. S.; Liu, L. Hollow cobalt phosphide octahedral pre-catalysts with exceptionally high intrinsic catalytic

activity for electro-oxidation of water and methanol. *J. Mater. Chem. A* **2018**, *6*, 20646–20652.